

Sorption mechanisms of lead on soil-derived black carbon formed under varying cultivation systems

Qingjie Zhao ^{a,1}, Jianhong Li ^{a,b,1}, Binoy Sarkar ^c, Weidong Wu ^a, Boling Li ^a, Ruichun Liu ^d, Mohsin Nawaz ^e, Muhammad Zia-ur-Rehman ^f, Hailong Wang ^{b,g,**}, Zhipeng Wu ^{a,*}

^a College of Tropical Crops, Hainan University, Haikou 570228, China

^b Biochar Engineering Technology Research Center of Guangdong Province, School of Environmental and Chemical Engineering, Foshan University, Foshan 528000, China

^c Lancaster Environment Centre, Lancaster University, Lancaster, LA1 4YQ, United Kingdom

^d Flood Control and Drought Relief Office of Hangjin County, Ordos 017400, China

^e Key Laboratory of Genetics and Germplasm Innovation of Tropical Special Forest Trees and Ornamental Plants, Ministry of Education, College of Forestry, Hainan University, Haikou 570228, China

^f Institute of Soil and Environmental Sciences, University of Agriculture, Faisalabad, 38040, Pakistan

^g Key Laboratory of Soil Contamination Bioremediation of Zhejiang Province, Zhejiang A&F University, Hangzhou 311300, China

* Corresponding author.

** Correspondence to: H. Wang, School of Environmental and Chemical Engineering, Foshan University, Foshan 528000, China

E-mail addresses: hailong.wang@fosu.edu.cn (H. Wang), peter@hainanu.edu.cn (Z. Wu).

¹ Qingjie Zhao and Jianhong Li contributed to the work equally and should be considered co-first authors.

24 **Highlights**

25 Cultivation intensities of soils significantly affect black carbon characteristics.

26 High cultivation intensity increased Pb in ion exchange fraction on black carbon.

27 Ion exchange and hydrogen bonded Pb fractions accounted for about 80% of total Pb.

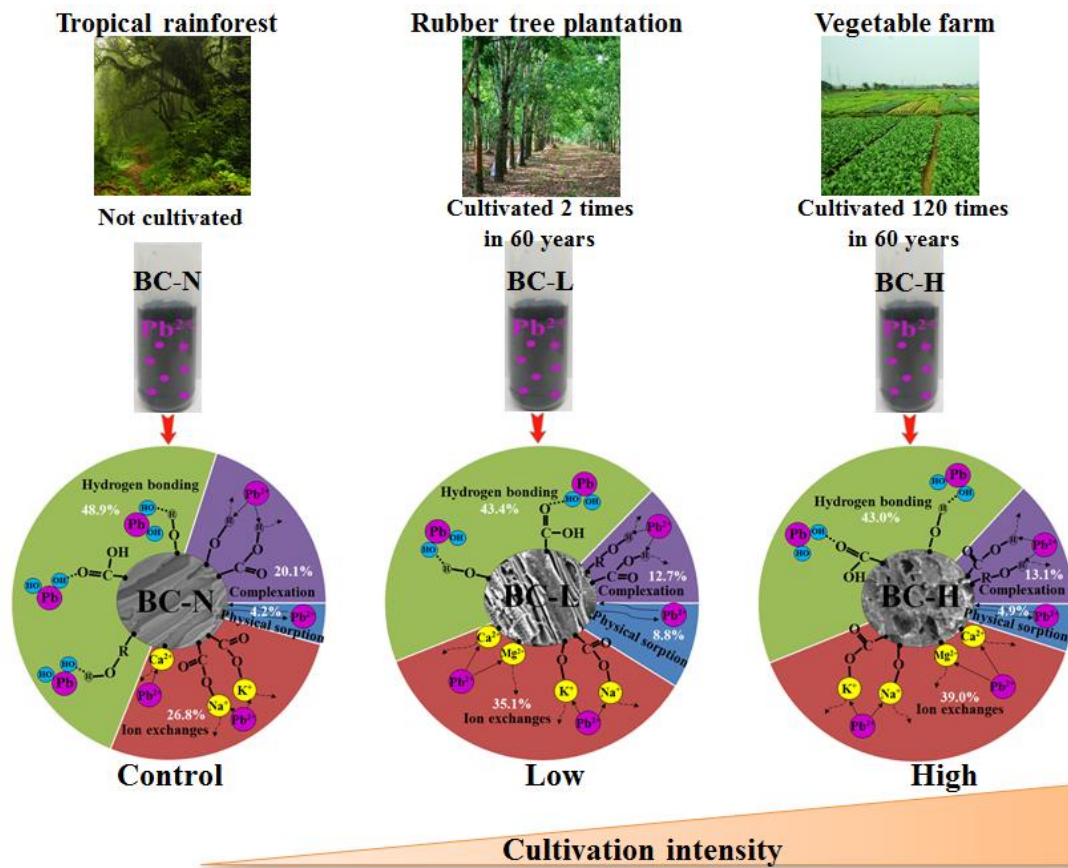
28 Black carbon had high potential to retain Pb in stable form (by 18.7 - 21.1 mg kg⁻¹).

29 Pb amount in ion exchange fraction was highly correlated with CEC of black carbon.

30

31 **Graphical abstract**

32



33

34

35 **Abstract**

36 The knowledge about lead (Pb) sorption on soil-derived black carbons (SBCs) under different cultivation
37 intensities of soils is limited. In this study, chemical and spectroscopic methods were applied to investigate the
38 Pb sorption mechanisms on SBCs in soils from a forest land, a rubber plantation area, and a vegetable farm with
39 none, less and highly intensive cultivation, respectively, that are located in the Hainan Island of China. Results
40 showed that the specific surface area and cation exchange capacity of the SBCs from the less and highly
41 intensive cultivation soils were 4.5- and 2.7-fold, and 1.3- and 1.8-fold higher compared to that of SBC from the
42 no-cultivation soil, which subsequently enhanced the Pb sorption capacities of SBCs in iron exchange fraction.
43 Ion exchange and hydrogen bonded Pb fractions together accounted for about 80% of total Pb sorbed on all
44 SBCs at an externally added 1,000 mg L⁻¹ Pb solution concentration. The O=C-O groups also played key roles
45 in Pb sorption by forming complexes of O=C-O-Pb-O and/or O=C-O-Pb. Overall, SBCs in soils under all
46 studied cultivation intensities showed high potential to sorb Pb (with the maximum absorbed Pb amount of 46.0
47 to 91.3 mg g⁻¹), and increased Pb sorption capacities of the studied soils by 18.7 - 21.1 mg kg⁻¹ in the stable
48 fraction (complexation). Therefore, SBC might be a potential environment-friendly material to enhance the Pb
49 immobilization capacity of soil.

50

51 **Keywords:** Aging of organic carbon; biochar; sequential desorption; TG/DTG; XPS.

52

53 **Abbreviations:** SBC: soil-derived black carbon; BC: black carbon; SOC: soil organic carbon; SSA: specific
54 surface area; CEC: cation exchange capacity; ICP-MS: inductively coupled plasma mass spectrometer; PTEs:
55 potentially toxic elements; TG/DTG: thermogravimetric and differential thermogravimetric; XPS: X-ray
56 photoelectron spectroscopy.

57

58 **1. Introduction**

59 Sorption of potentially toxic elements (PTEs) on solid matrices such as soils and sediments is one of the key
60 components which determine the fate and behavior of PTEs in the environment (Chiou, 2002; Shaheen et al.,
61 2013). It has been recognized that various forms of soil organic matter (SOM) could serve as dominant
62 environmental “compartments” for the sorption and accumulation of PTEs (Zhou et al., 2018). Black carbon
63 (BC) serves as a chemically and biologically stable form of SOM which exists in the soil over a long period
64 (Liang et al., 2008; Qi et al., 2017). As one form of BCs, biochar has been found to be an excellent material for
65 adsorption of organic pollutants (Qin et al., 2018; Zhang et al., 2019; Chen et al., 2020a) and PTEs (Ali et al.,
66 2020; Imran et al., 2020; Yin et al., 2020). The BC may significantly affect the sorption and immobilization of
67 PTEs in soils in a wide range of biogeochemical processes (Liang et al., 2006; Qi et al., 2017), and could be
68 regarded as an eco-friendly and potential material to immobilize PTEs in soil (Nie et al., 2018; Bandara et al.,
69 2020; Wei et al., 2020). Therefore, the sorption capacity and the specific mechanisms of BC for metal ion
70 retention are of great importance in remediation of contaminated soils.

71 Biomass-derived BC exists ubiquitously in soils to varying extents as a result of deliberate vegetation
72 burning, wildfires or emissions from energy production units (Schmidt and Noack, 2000). For example, the
73 2019-20 fire season in eastern Australia is attracting considerable international attention where millions of ha of
74 temperate forest areas have been burnt during the fire (Nolan et al., 2020). It has caused serious ecological
75 damage, along with that a large amount of charcoal, the product of the incomplete combustion of vegetation
76 (Pereira et al., 2014), was produced. Aging of charcoals (a fraction of BCs) in the soil results in the formation of
77 persistent soil organic carbon (SOC) (Bennett et al., 2020), including soil-derived black carbon (SBC). The
78 SBCs from natural formation or artificial amendments, however, have high specific surface area (SSA), high
79 cation exchange capacity (CEC), and various organic functional groups. These characteristics might increase the

80 sorption capacity of PTEs on SBC during the PTE remediation processes (Qi et al., 2017). In recent years,
81 artificial BC such as biochar has been successfully applied as a highly efficient soil amendment to immobilize
82 PTEs (Liu et al., 2018; Li et al., 2019a; Li et al., 2020).

83 Exploration of the sorption and immobilization potential of PTEs by natural BC in soils is also immensely
84 important since the global BC stock in waters, sediments, and soils combined is 300 to 500 giga-metric tons of
85 carbon (Jaffé et al., 2013). Previous studies reported that aging of biochar following soil application changes its
86 physiochemical properties while forming a range of biochar-derived organic materials (Mia et al., 2017).
87 Moreover, crop cultivation practices can increase the association of charcoal with soil minerals, e.g., silicates,
88 phosphates, aluminum oxides, and iron oxides in soils, thereby changing the elemental characteristics of
89 charcoal (Hardy et al., 2017). The above changes in elemental compositions cause a modification of the
90 physiochemical properties of charcoals and BC affecting their capacity to immobilize PTEs (Bandara et al.,
91 2020). Few studies also claim that intensive cultivation of soils can change the PTE retention efficiency of SBC
92 (Zahedifar, 2017).

93 It is difficult for agricultural and forestry soils to avoid PTE pollution in the process of land development
94 and utilization due to a rapid development of social economy, industry and urbanization. Unraveling the sorption
95 characteristics and mechanisms of PTEs on SBC from agricultural and forestry soils can help exploring the
96 potential of BC or biochar in influencing the immobilization of PTEs in agricultural and forestry lands. The
97 natural tropical rainforest in the Bawangling Forest Region (108.88°-109.33°E, 18.86°-19.20°N) of Hainan
98 island in China (Lu et al., 2018) was rarely disturbed for replacing its plantations, and has therefore existed for
99 several thousand years without any cultivation (Zhang et al., 2010; Wang et al., 2017a), except a serious damage
100 caused by people for creating more farmland or for obtaining more forest resources about 600 years ago in the
101 Ming Dynasty (Dodson et al., 2019). The lands nearby the Bawangling Forest Region have been cultivated for

102 about 60 years (Lu et al., 2018). Rubber trees near the Bawangling Forest Region was adopted as the secondary
103 plantation under less intensive cultivation (cultivated about 20 years ago) system, while vegetables were grown
104 twice a year in some lands under highly intensive cultivation system. It could be hypothesized that the
105 physicochemical properties (e.g., CEC, elemental composition and organic functional groups) of SBCs under
106 the less intensive cultivation system would be significantly different from those of the highly intensive
107 cultivation system and no cultivation system, which would further affect the sorption capacities and mechanisms
108 of Pb (a representative PTE) by SBCs from these systems.

109 The sorption mechanisms of PTEs on artificial BC (e.g., biochar) in aqueous solutions have been reported
110 extensively (Li et al., 2019b; Yang et al., 2019; Fang et al., 2020). The major mechanisms involved in the
111 removal of PTEs from aqueous solutions using biochars were ion-exchange, electrostatic attraction, outer-sphere
112 and/or inner-sphere complexation, surface precipitation and/or co-precipitation (Wang et al., 2019). Several
113 methods including potentiometric titration, sequential extraction, thermal analysis techniques such as
114 thermogravimetric (TG) and differential thermogravimetric (DTG) analyses, and X-ray photoelectron
115 spectroscopy (XPS) have been proven as useful methods to study the characteristics of organic functional
116 groups and thermal stability of organic components on BCs, and analyze the interactions between carbon-based
117 adsorbents and PTE adsorbates (Plante et al., 2009; Li et al., 2019b; Xia et al., 2019). These methods were used
118 to investigate Pb sorption characteristics and mechanisms of SBCs from different soils in the current study.

119 In this study, we separated three SBCs from the soils under different cultivation systems (i.e., no-cultivation,
120 less intensive cultivation, and highly intensive cultivation) in the Hainan island of China to conduct Pb sorption
121 and desorption experiments on SBCs. The specific objectives of this work are to: (1) characterize the elemental
122 composition and physicochemical properties of the SBCs; (2) explore sorption and desorption characteristics of
123 SBCs for Pb; and (3) investigate the sorption mechanisms of Pb onto SBCs.

124

125 **2. Materials and methods**

126 **2.1. Soil collection and separation of black carbon**

127 Three surface soils (0–20 cm depth) were collected in triplicate from the three sampling sites (without any
128 artificial black carbon added), including a natural tropical rainforest (109.09°E, 19.13°N) in the Bawangling
129 Forest Region (Hainan Province of China), a rubber tree plantation area (109.50°E, 19.53°N), and a vegetable
130 farm (109.57°E, 19.48°N) near the Bawangling Forest Region. The three collected soil samples represented
131 no-cultivation, less intensive cultivation and highly intensive cultivation systems, respectively, and referred to as
132 Soil 1, Soil 2 and Soil 3. Following sample collection, soil pH was determined in a soil suspension (soil:water =
133 1:2.5(w/v)) according to Li et al. (2020), while soil organic carbon was determined using the $K_2Cr_2O_7$ method
134 (Bao, 2000). The pH value of Soil 1, Soil 2 and Soil 3 was 4.53, 4.98 and 4.64, while the soil organic carbon
135 content was 31.01, 12.15 and 9.10 g kg⁻¹, respectively. The clay, silt, and sand particles were 13, 24 and 63%,
136 and 18, 37 and 45% in Soil 1 and Soil 2, respectively. The soil particle fractions with particle size less than 10
137 μ m, between 10 and 50 μ m, and greater than 250 μ m were 33.0, 23.2 and 43.8%, 40.8, 29.4 and 29.8%, and 13.7,
138 56.8 and 29.5% in Soil 1, Soil 2 and Soil 3, respectively.

139 The SBC particles (with diameter > 0.5 mm) were selected and picked from Soil 1 (no-cultivation), Soil 2
140 (less intensive cultivation) and Soil 3 (highly intensive cultivation) using superfine stainless forceps according
141 to Dong et al. (2017), and referred to as BC-N, BC-L and BC-H, respectively. The SBC particles were
142 suspended into deionized water at a ratio of 1:10 (w/v) and shaken slightly to remove soil particles adhered to
143 the SBC particles. The SBC particles were then washed three times with deionized water, and put in a 60 °C
144 drying oven until the weight of the particles reached a constant value (Koide et al., 2011). All SBC particles
145 were ground and passed through a 0.15 mm sieve, and stored for further use.

146

147 **2.2. Preparation of Pb-loaded black carbon**

148 Lead-loaded SBCs were prepared by adding 1.0 g of SBC into 500 mL of 10, 20, 40, 80, 150, 300, 600 and
149 1000 mg L⁻¹ of Pb aqueous solutions (by dissolving analytical grade Pb(NO₃)₂) at pH 5.0 in Erlenmeyer flasks.
150 Uzun et al. (2003) reported Pb precipitation (Pb(OH)₂) at pH 5.5. In this study, the pH value of solutions was
151 selected at 5.0 since the pH of the studied soils ranged from 4.5 to 5.0. The flasks were capped with rubber plugs,
152 agitated on a thermostatic reciprocating shaker at 220 rpm (25 °C) for 24 h. Then, the aqueous solutions were
153 filtered through a 0.45 µm cellulose-acetate membrane filter paper, and the residual Pb-loaded SBCs was
154 washed with deionized water, and air-dried at room temperature prior to further analysis.

155

156 **2.3. Characterization of black carbon**

157 Total hydrogen (H), carbon (C), and nitrogen (N) contents of SBCs were measured using an elemental
158 analyzer (Vario ELIII - Elementary Company, Germany). The oxygen (O) content was calculated by the
159 difference assuming that the SBC was composed only of H, C, N, and O (Wu et al. 2012). Ash content of the
160 SBCs was determined by placing crucibles containing the samples in a muffle furnace at 750°C for 6 h
161 (D1762-84, 2007). The crucibles were kept with lids in a desiccator for 1 h for cooling, and then weighed. Pore
162 volume and SSA of SBCs were measured by N₂ adsorption isotherms (ASAP2460, Micromeritics, USA)
163 applying the Brunauer-Emmett-Teller (BET) equation (Brunauer et al., 1938). The contents of acidic functional
164 groups of SBCs were determined by the Boehm titration method (Boehm, 1994). The CEC of SBCs was
165 determined following 1 M ammonium acetate (pH 7) extraction method (Wu et al., 2017). In order to measure
166 total carbon content of SBCs in soils, soil samples were digested using peroxide to remove non-BC. Twenty
167 grams of air-dried soil was treated with 30% (w/w) peroxide (initially 10 mL, with daily additions up to a total

168 of 30–50 mL until no further bubbles appeared), and heated on a hot plate at 90 °C to ensure maximum non-BC
169 removal (Liang et al., 2006). Total carbon content of SBCs in soils was then measured using the
170 $K_2Cr_2O_7$ -heating method (Bao, 2000). The total carbon content of BC-N, BC-L and BC-H in Soil 1, Soil 2 and
171 Soil 3 was 0.81, 1.58 and 1.08 g kg⁻¹, therefore, the weight content of BC-N, BC-L and BC-H in the soils was
172 1.65, 3.30 and 2.36 g kg⁻¹, respectively ($W_{BC} = T_{BC} \times E_{C\%}$, while W_{BC} , T_{BC} and $E_{C\%}$ refer to weight content of
173 SBCs in soils, total carbon content of SBCs in soils, and carbon percentage of SBCs, respectively).

174 Thermogravimetric (TG) and differential thermogravimetric (DTG) analyses curves were obtained using a
175 thermogravimetric analyzer (SDT Q600, TA Instruments, USA) at a heating rate of 10 °C min⁻¹ from 30 °C to
176 1000 °C under a controlled atmosphere of N₂ (50 mL min⁻¹) with an initial material mass of 30 mg. Fourier
177 transform infrared (FTIR) analysis of SBCs before Pb sorption was conducted according to Wu et al. (2016).
178 Spectra were collected using a TENSOR 27 FTIR spectrophotometer (Bruker Company, Germany) scanning
179 from 4000 to 400 cm⁻¹ (wavenumber) at a resolution of 2 cm⁻¹. The X-ray photoelectron spectroscopy (XPS,
180 AXIS SUPRA, Japan) was used to measure the bonding energies of C, O, and Pb on the SBCs and Pb-loaded
181 SBCs prepared at 1000 mg L⁻¹ Pb aqueous solution (scans for C 1s, O 1s and Pb 4f). Samples were freeze-dried,
182 ground to powder in the anaerobic chamber, and pressed into pellets. The energy range was 0–1000 eV for
183 wide-scan spectra (Li et al., 2020).

184

185 **2.4. Sorption experiments**

186 A stock solution of 1000 mg L⁻¹ Pb was prepared by dissolving Pb(NO₃)₂ in 0.01 M NaNO₃ solution.
187 Sorption kinetics was determined by determining sorption amounts at various time intervals (5, 10, 15, 20, 30,
188 40, 60, 120, 240, 480, 960 and 1440 min) at pH 5.0. The pH value of suspension was adjusted with 0.1 M NaOH
189 or 0.1 M HNO₃ solution to simulate a typical soil water situation (Li et al., 2019b). Sorption isotherm

190 experiments were carried out with different initial Pb concentrations (10, 20, 40, 80, 150, 300, 600 and 1000 mg
191 L⁻¹) at pH 5.0. Both sorption kinetics and isotherm experiments involved an adsorbent suspension with a
192 SBC:solution ratio of 1:25 (w/v) in 50 mL tubes (Wu et al., 2017). These tubes were agitated on a rotating
193 shaker at 220 rpm and 25 °C for 24 h. The solutions were filtered (< 0.45 µm filter) and preserved in test tubes
194 (Li et al., 2019b). Concentrations of Pb in the filtrates were measured using an inductively coupled plasma mass
195 spectrometer (ICP-MS, Thermo Fisher-X series, USA). The released alkali or alkaline earth metals (such as Na⁺,
196 K⁺, Mg²⁺ and Ca²⁺) from the original SBCs in the supernatant (under Pb concentration of 1000 mg L⁻¹) were
197 also analyzed by ICP-MS. The corresponding release of Na⁺, K⁺, Mg²⁺ and Ca²⁺ from the SBCs with deionized
198 water (at the same pH) served as the control. All treatments in the sorption experiments were conducted in
199 triplicate.

200

201 **2.5. Desorption experiments**

202 Lead fractionation in Pb-loaded SBCs (prepared in section 2.2 of this study) during desorption experiments
203 was conducted using the method modified from Andreas and Zhang (2014). The sorbed Pb was fractionated into
204 (i) physical sorption, (ii) ion exchange, (iii) hydrogen bonding, and (iv) complexation fractions. The physical
205 sorption fraction is affected by van der Waals force between Pb and SBC surface, ion exchange fraction is
206 attributed to the cation exchange between Pb and other cations on SBC surface, hydrogen bonding fraction is
207 formed by hydrogen bonds between Pb forming hydrates [Pb(H₂O)₆²⁺] and oxygen-containing functional groups
208 on SBC surface, and complexation fraction is influenced by coordination reaction of Pb on SBCs surface
209 (Andreas and Zhang, 2014). Accordingly, 0.05 g of Pb-loaded SBC was added into a 50 mL plastic tube. All
210 tubes with samples were placed on a reciprocating shaker at 25 °C and rotated at 220 rpm, and then sequentially
211 extracted with (i) 25 mL ultrapure water shaking for 2 h, (ii) 8 mL CH₃COONH₄ (1 M, pH=7) shaking for 6 h,

212 (iii) 10 mL CH₃COOH (4.37 M) + NH₂OH·HCl (0.04 M) shaking for 5 h, and (iv) 10 mL sodium
213 pyrophosphate (0.1 M) shaking for 5 h, respectively, to determine the above four Pb fractions. The suspensions
214 were centrifuged at 5000 rpm for 20 min (at 25 °C) using a centrifuge machine (H2050R, Cence, China), and
215 filtered using 0.45 μm cellulose-acetate membrane filters. Lead concentrations in the filtrates were measured
216 using ICP-MS.

217 The sorption kinetics of Pb onto SBC was analyzed by the pseudo-first-order and pseudo-second-order
218 models, the sorption isotherms of Pb onto SBCs were analyzed by the Langmuir and Freundlich models (Text
219 S1 of the Supporting Information).

220 The Pb sorption capacity of the SBCs in physical sorption fraction (Q_{phy}), ion exchange fraction (Q_{exc}),
221 hydrogen bonding fraction (bond with oxygen-containing function groups, Q_{hyd}), complexation fraction (Q_{com})
222 and total sorption fraction (Q_{tot}) were calculated by the Langmuir model fitting.

223

224 **2.6. Statistical analysis**

225 Results were expressed on a dry mass basis, and shown as mean ± standard deviation (SD) of three
226 replicates per treatment. The standard deviation bars of results were added in specific figures. The fitting of the
227 Langmuir and Freundlich models, pseudo-first-order and pseudo-second-order models, and the graphing of XPS
228 spectra were done using the software Origin 9.0 (Origin Lab, USA).

229

230 **3. Results and discussion**

231 **3.1. Properties of soil-derived black carbons**

232 Elemental properties of the SBCs are shown in Table 1. The N content of SBCs increased 1.25- and
233 2.23-fold in Soil 2 (BC-L) and Soil 3 (BC-H) under the low and high cultivation intensity compared to that in

234 Soil 1 (BC-N) under no cultivation (the control). Values were presented by 1.64 and 2.36% N contents of BC-L
235 and BC-H, respectively, while 0.73% for BC-N (the control). The H and O contents of SBCs were slightly
236 increased with the increasing cultivation intensity from the control (3.61 and 46.5%) to low (3.87 and 46.6%)
237 and high (3.90 and 47.8%) (Table 1). However, the C content slightly decreased (49.1, 47.9 and 45.9% C
238 contents of BC-N, BC-L and BC-H, respectively) under the elevated cultivation intensity (Table 1). This might
239 be attributed to the enhanced disturbances of soils and weathering of SBCs by various cultivation practices, e.g.,
240 ploughing, wetting and drying, and water and fertilizer management (Hardy et al., 2017). During farming of the
241 land, the above practices inputted more N into the soil than the no-cultivation system, and accelerated the
242 decomposition of BCs in the soil by bringing down the C:N ratio (Hardy et al., 2017). As a result, labile
243 C-containing groups such as aromatic and aliphatic groups of SBCs were decomposed by microorganisms
244 (Kuzuyakov et al., 2009). Meanwhile, an increasing proportion of H and O-rich functional groups such as
245 carboxyl, carbonyl and O-alkyl were formed on SBCs during the BC mineralization (Kuzuyakov et al., 2009; Mia
246 et al., 2017). Additionally, a high proportion of N-containing groups could increase the reaction ratio of
247 positively charged N-containing functional groups in soil to negatively charged C-containing functional groups
248 on SBCs under a high cultivation intensity (Hardy et al., 2017; Mia et al., 2017; Wang et al., 2018). This might
249 contribute to the increase in N content of SBCs with increasing soil cultivation intensity. Similarly, Hardy et al.
250 (2017) reported that charcoal in cropland over long cultivation time had higher O and H contents and N-alkyl
251 groups than short cultivation duration due to enhanced weathering of various C substrates.

252 The higher the ratio of H/C and O/C in SBC, the lower is the aromaticity of SBC, and the more abundant is
253 the organic functional groups such as hydroxyl and carboxyl groups (Wu et al., 2012; Wu et al., 2016). The
254 order of H/C and O/C ratios of SBCs was: BC-H > BC-L > BC-N (Table 1). Thus, the H/C and O/C ratios
255 increased under elevated weathering and cultivation disturbances of SBCs. These might be attributed to the

256 increased phenol, carbonyl and carboxyl functional groups which were created by the oxidation of SBC surfaces
257 during the aging of BCs under high cultivation intensity (Cao et al., 2019). The total content of acidic functional
258 groups (the sum of carboxylic acid (RCOOH), weak acid ester (RCOR'), and phenolic hydroxyl groups (AOH))
259 in BC-H (1.70 mmol g⁻¹) and BC-L (1.71 mmol g⁻¹) was higher than that of BC-N (1.57 mmol g⁻¹; Table 1),
260 which also indicated that hydroxylation and carboxylation of SBCs could be enhanced by increased cultivation
261 intensity and aging. As reported by Mukherjee et al. (2014), the advanced oxidation of SBCs most likely created
262 phenol, carboxyl and carbonyl functional groups at the edge of aromatic rings on the surfaces. Mia et al. (2017)
263 found that progressive aging of biochar (artificial BC) also led to a gradual formation of surface functional
264 groups such as phenolic, carboxyl, and carbonyl groups. The results of this study are consistent with those of
265 previous studies, showing that aging of charcoals in soil resulted in the oxidation of their surfaces (Lehmann et
266 al., 2005; Hardy et al., 2017). Accordingly, both H/C and O/C ratios of charcoal could be increased through
267 elevated aging intensities (Cheng et al., 2008; Pereira et al., 2014).

268 The CEC of three SBCs ranged from 128–227 cmol kg⁻¹ (Table 1) with the order of BC-H (227.3 cmol
269 kg⁻¹) > BC-L (166.4 cmol kg⁻¹) > BC-N (128 cmol kg⁻¹). Under the low and high cultivation intensity of the
270 soils, a gradual aging resulted in the value of SSA of BC-L and BC-H to be 4.5- and 2.7-fold higher than that of
271 BC-N (Table 1). Thus, more sorption sites might be presented on the surface of BC-L and BC-H than BC-N,
272 which could increase CEC of SBCs. The higher total content of acidic functional groups of BC-L and BC-H
273 might also be responsible for the increase in CEC compared to that of BC-N in this study. Similarly, previous
274 studies reported that CEC of charcoal increased over increasing aging intensity (Cheng et al., 2008). The CEC,
275 variety of active functional groups and SSA were reported to affect the sorption capacities of biochar toward
276 PTEs, including Pb sorption and immobilization (Lu et al., 2017; Wu et al., 2017; Li et al., 2019b).

277 The peak intensity of functional groups on SBCs including the aromatic ring C=O stretching of β -diketone

278 ligands (1620–1580 cm^{-1}) (Li et al., 2019b), and cyclic anhydride C–O–C stretching (1300–1199 cm^{-1}) (Li et
279 al., 2019b; Mumtaz et al., 2019) vibrations decreased with increasing cultivation intensity (Fig. 1), while the
280 intensity of aliphatic C–H asymmetric stretching (2920 cm^{-1}), R–CH₃ symmetric stretching (2850 cm^{-1}) (Chen
281 et al., 2020b), and non-cyclic anhydride C–O–C stretching (1150–1060 cm^{-1}) vibrations increased (Fig. 1).
282 These changes were contributed likely by the hydrolyzation or decomposition of cyclic anhydride of carboxylic
283 acid, and formation of C–H and R–CH₃ contained functional groups on SBCs during the increased cultivation
284 intensity of the soils.

285

286 **3.2. Sorption and desorption of Pb from Pb-loaded SBCs**

287 The kinetics of Pb sorption on the three SBCs at pH of 5.0 are presented in Fig. S1 (Supporting Information).
288 The sorption kinetics of Pb on the three SBCs were expressed well by the pseudo-second-order model, rather
289 than pseudo-first-order model, which was indicated by their respective r^2 values (Table S1). About three hours
290 was required for Pb sorption on the three BCs to reach the equilibrium likely through predominant
291 chemisorption processes (Lu et al., 2012; Bandara et al., 2020).

292 The sorption isotherms of Pb on BC-N and BC-H were interpreted by the Langmuir model with r^2 values of
293 0.981 and 0.920, respectively (Table S2, Fig. 2). Fitting of sorption data to the Langmuir model indicated that
294 the Pb sorption on BC-N and BC-H occurred mainly through surface monolayer interactions (Wu et al., 2017).
295 However, the Freundlich model provided a better fit than the Langmuir model for BC-L with a r^2 value of 0.925
296 (Table S2, Fig. 2), which indicated that the Pb sorption on BC-L was predominated by a multilayer sorption
297 process (Xia et al., 2019).

298 The maximum Langmuir sorption capacity values of Pb on BC-N, BC-L and BC-H under the same
299 experimental conditions were 75.6, 46.0 and 91.3 mg g^{-1} , respectively. Only a few previous studies reported the

300 sorption of Pb on SBC. Wang et al. (2011) showed that the wheat-residue derived BC could sorb Pb up to 0.65
301 mmol g⁻¹ (equal to 134 mg g⁻¹) at Pb concentration of 20 mmol L⁻¹. The sorption capacity of wheat-residue
302 derived BC was higher than that of the three SBCs in this study. However, the maximum amount of Pb sorption
303 to biochar (artificial BC) produced from different agricultural biomass might range from 13.1 to 88.7 mg g⁻¹
304 (Table S3). Unraveling the sorption mechanisms of Pb to different SBCs can help to understand the difference in
305 the sorption capacities of SBCs for Pb. The exact Pb fractions on Pb-loaded SBCs would be able to reveal the
306 related sorption mechanisms of Pb to SBCs.

307 In the desorption experiments, the total Pb amount (Q_{tot}) and Pb amount of four sorbed fractions, e.g.,
308 physical sorption (Q_{phy}), ion exchange (Q_{exc}), hydrogen bonding (Q_{hyd}) and complexation (Q_{com}) fractions are
309 shown in Fig. 3. With the increase of initial concentration of Pb, the amount of Pb in Q_{phy} , Q_{com} , Q_{hyd} , and Q_{exc}
310 fractions reached the sorption equilibrium successively, indicating that the exact saturation order of the four Pb
311 fractions was Q_{phy} , Q_{com} , Q_{hyd} , and Q_{exc} . The Q_{exc} , Q_{hyd} , Q_{com} and Q_{tot} on the three types of Pb-loaded SBCs were
312 all found to be well fitted to the Langmuir model (Table S4) with high r^2 values ranging from 0.971 to 0.987,
313 which was attributed to the fact that Pb desorption from Pb-loaded SBCs was a reverse process on Pb sorption
314 to SBCs (Andreas and Zhang, 2014).

315 The percentage of sorbed Pb in Q_{hyd} and Q_{com} fractions of Pb-loaded SBCs (at Pb concentration of 1000 mg
316 L⁻¹) significantly decreased from 48.9 and 20.1% to 43.4 and 12.7% under no-cultivation in comparison to the
317 low cultivation intensity, while decreased to 43.0 and 13.1% under high cultivation intensity (Fig. 4). The
318 percentage of Pb in the Q_{exc} fraction on SBCs however increased from 26.8% to 35.1 and 39.0%, respectively,
319 from no-cultivation to low and high cultivation intensities. Results showed that Q_{exc} and Q_{hyd} were the two most
320 important Pb fractions on the three Pb-loaded SBCs. The sum of Pb amounts in Q_{exc} and Q_{hyd} of the three
321 Pb-loaded SBCs was ranging from 35.2 to 56.1 mg g⁻¹, and accounting for 75.7 to 82.0% of total sorbed Pb

322 (Table S5 and Fig. 4). Previous research also reported that biochar could remove metal ions from aqueous
323 solutions by various mechanisms including electrostatic attraction, complex formation, reduction and
324 precipitation (Lu et al., 2012; Li et al., 2019b). Similarly, Andreas and Zhang (2014) reported that metal sorption
325 onto soil-derived humin (a specific organic matter) in freshwater media was dominated by hydrogen bonding
326 and ion exchange fractions.

327 The content of BC-N, BC-L and BC-H in the soils was 2.85, 5.69 and 4.07 g kg⁻¹, while Pb amount in the
328 Q_{com} fraction of these Pb-loaded SBCs was 11.52, 5.68 and 8.95 mg g⁻¹, respectively (Table S5 and Fig. 4). The
329 complexation (Q_{com}) fraction of Pb was presented to be stable since the extracting agents such as ultrapure water,
330 CH₃COONH₄ (1 M, pH=7), CH₃COOH (4.37 M) and NH₂OH·HCl (0.04 M) could not extract this Pb fraction
331 (Andreas and Zhang, 2014) from the Pb-loaded SBCs. Therefore, we inferred that the BC-N, BC-L and BC-H
332 might increase the capacity of Soil 1, Soil 2 and Soil 3 to adsorb Pb as a stable (complexation) fraction by 19.0,
333 18.7 and 21.1 mg kg⁻¹ (Table S5), respectively.

334

335 **3.3. Sorption mechanisms of Pb to SBCs**

336 It was reported that the efficacy of various biochars derived from different biomass materials to adsorb PTE
337 contaminants depends on its properties, e.g., surface area, pore size distribution, ion-exchange capacity (Bandara
338 et al., 2020) and surface oxygen-containing functional groups (Xia et al., 2019) representing different sorption
339 mechanisms. Accordingly, the sorption mechanisms of Pb onto SBCs were divided into the following four parts.

340 (1) Physical sorption: The orders of Q_{phy} on Pb-loaded SBCs and SSA of SBCs were both in the order:
341 BC-L > BC-H > BC-N (Table S5 and Table 1), while the SSA values of SBCs was highly correlated to Q_{phy}
342 fractions on Pb-loaded SBCs with a correlation coefficient (R²) value of 0.94 (Fig. S2a). Similar results were
343 reported by Zhang et al. (2019) who realized that the surface area of a sludge-based biochar was improved after

344 activation by different activators, thus improving its physical Pb sorption capacity. Moreover, Ngambia et al.
345 (2019) found that tunnels on the rods of sludge derived carbon provided a high surface area, extra sorption sites
346 and interspace for easy contamination diffusion contributing to surface physical adsorption.

347 (2) Ion exchange: The CEC values of SBCs were highly correlated to the Q_{exe} fractions of Pb-loaded SBCs
348 with a correlation coefficient (R^2) of 0.833 (Fig. S2b). Moreover, the CEC values of SBCs and Q_{exe} fractions of
349 Pb on Pb-loaded SBCs all followed the order: BC-H > BC-L > BC-N (Table S5 and Table 1). Therefore, the Q_{exe}
350 fraction of Pb-loaded SBCs might be mainly attributed to the cation exchange mechanism of Pb sorption on
351 SBCs.

352 The sum amounts of Na^+ , K^+ , Mg^{2+} and Ca^{2+} released in the supernatants after Pb sorption onto BC-N, BC-L
353 and BC-H were equivalent to 13.3, 15.6 and 18.6 mg Pb g^{-1} , accounting for 23.1, 34.9 and 27.2% of the total Pb
354 sorbed by BC-N, BC-L and BC-H (prepared under Pb concentration of 1000 mg L^{-1}), respectively (Table S6).
355 The sum amounts of Na^+ and K^+ (mono-valent cations), which could be related to the electrostatic ion exchange
356 with Pb (Lu et al., 2012) since they cannot form precipitates or be coordinated with surface functional groups of
357 BCs, were equivalent to 5.32, 3.0 and 3.67 mg Pb g^{-1} accounting for 34.5, 19.1 and 13.8% of the Q_{exc} values on
358 Pb-loaded BC-N, BC-L and BC-H, respectively (Table S6). Meanwhile, the sum amounts of Mg^{2+} and Ca^{2+}
359 (divalent alkaline earth cations), which could originate from the exchange sites of inorganic minerals and the
360 chelated surface functional groups such as R-COO-Me or R-O-Me on SBCs, were equivalent to 7.95, 12.6 and
361 15.0 mg Pb g^{-1} accounting for 51.6, 80.2 and 56.1% of the Q_{exc} , respectively (Table S6). Our results showed that
362 the exchange sites adsorbed or chelated Pb fractions in Q_{exc} of Pb-loaded SBCs were far more than that of the
363 electrostatically ion exchanged Pb fraction, indicating that chelation might have played a more important role
364 during the sorption process (Lu et al., 2012). Similar result was reported by Li et al. (2019b) that ion exchange
365 was the main mechanism for Pb sorption by coconut-fiber biochar with electrostatic ion exchange and chelation

366 processes.

367 (3) Hydrogen bonding: The results of TG and DTG thermograms of the three SBCs are shown in Fig. S3.
368 The TG and DTG analyses detected three endothermic peaks between 30 and 180 °C, 300 and 350 °C, and 380
369 and 560 °C for all samples (Fig. S3). Previous studies ascribed the endothermic peak at temperatures below
370 200 °C to the loss of adsorbed water, while that near 325 °C to decarboxylation (volatilization of –COOH) and
371 further dehydroxylation (volatilization of –OH) of surface organic functional groups, and that around 475 °C to
372 the thermal reaction of the aromatic nuclei of organic matter (Plante et al., 2009). Carbohydrates and other
373 aliphatic compounds would be pyrolyzed at 300 to 350 °C in the TG analysis (Plante et al., 2009), the weight
374 loss of SBCs (Fig. S3; attributed to volatilization of –COOH and –OH), however, were highly correlated to the
375 sum content of AOH and RCOOH groups (Table 1) with a R^2 value of 0.966 (Fig. S2c).

376 Moreover, the sum contents of AOH and RCOOH of SBCs were significantly correlated with Pb amount in
377 the Q_{hyd} fraction (with a R^2 value of 0.833; Fig. S2d). This might be attributed to the activities of –COOH and
378 –OH groups to adsorb Pb in aqueous solution through hydrogen bonding. It was reported that Pb would be
379 present mainly as the species of Pb^{2+} at pH 4 in aqueous solution, then the amount of Pb^{2+} would decrease with
380 an increase of pH to 5.5 due to $Pb(OH)^+$ formation (Ucun et al., 2003). Ucun et al. (2003) observed Pb
381 precipitation ($Pb(OH)_2$) when the initial pH of a biosorption medium was adjusted to pH 5.5. Thus, Pb^{2+} and
382 $Pb(OH)^+$ were likely to be adsorbed onto SBCs through hydrogen bonding at pH 5.0 as the Q_{hyd} fraction in this
383 study.

384 (4) Complexation: In order to elucidate the complexation mechanism, the XPS spectra of C and O groups on
385 the surface of SBCs with and without Pb loading were obtained for C 1s, O 1s and Pb 4f regions, and the
386 corresponding changes in the functional groups were determined (Fig. 5 and Table 2). The peak at the binding
387 energy of Pb 4f between 138 and 143 eV was found in all Pb-loaded SBC samples (Fig. 5b), which confirmed

388 that Pb was successfully complexed by the functional groups on SBCs. The binding energy of Pb 4f_{5/2} and
389 4f_{7/2} on Pb-loaded SBCs decreased to 143.79 eV and 138.89 eV in comparison with Pb(NO₃)₂ that centered at
390 145.0 eV and 139.9 eV (Batusaitis et al., 2012; Xin et al., 2012), respectively, indicating the presence of strong
391 affinity between SBC and Pb ions by newly formed Pb–O groups (Zhang et al., 2017).

392 As shown in Fig. 5c–h, three principal C species, i.e., C–C/C=C/C–H (hydrocarbon) at 284.7 eV, C–O
393 (aromatic) at 286.4 eV and C=O/O–C=O (carboxylic carbon) at 288.4 eV, and two O species such as C–O at
394 531.9 eV and C=O at 532.8 eV were identified in the three SBC samples (Deng et al. 2017; Xia et al., 2019). After
395 Pb sorption, the peak intensities of C–O (aromatic) significantly decreased, while that of O=C–O (carboxylic
396 carbon) and C=O significantly increased (Table 2). These results indicated that O=C–O groups played key roles
397 in Pb sorption by forming complexes of O=C–O–Pb and/or O=C–O–Pb–O (Yamada et al., 2014; Wang et al.,
398 2015).

399 Overall, the above four mechanisms all likely attributed to Pb sorption onto SBCs, while they had various
400 degrees of contributions. However, the amount of Pb adsorbed onto SBCs was dominated by the ion exchange,
401 hydrogen bonding and complexation fractions. The amount of Pb in the physical sorption, ion exchange and
402 hydrogen bonding fractions on Pb-loaded SBCs were highly correlated with SSA, CEC and the sum contents of
403 hydroxyl and carboxyl functional groups on SBCs, respectively.

404

405 **4. Conclusions**

406 The amount of Pb adsorbed onto different SBCs was dominated by the ion exchange and hydrogen bonded
407 fractions, which together accounted for about 80% of the total sorbed Pb, and was mainly attributed to CEC and
408 hydrogen bonding capacities of free carboxyl and hydroxyl groups of SBCs. The increased cultivation intensity
409 and aging of SBCs increased the H/C, O/C ratios and CEC of the SBCs compared to that with no cultivation.

410 Therefore, the Pb sorption capacity of SBCs in the ion exchange fraction increased with the increasing
411 cultivation intensity of soils. The maximum Pb sorption capacities of SBCs in this study were as high as that of
412 biochars produced from various agricultural biomasses. Moreover, the SBCs might increase the Pb sorption
413 capacities of the studied soils by 18.7 - 21.1 mg kg⁻¹ in stable fractions, which might not be released readily.
414 Overall, SBCs in soils under all studied cultivation intensities showed high potential to sorb and retain Pb in a
415 stable form. Increasing SBC content in soil during land management and utilization could befittingly be an
416 environment-friendly method to enhance the potential Pb immobilization capacity of soils. Further research
417 should be carried out to determine the PTE sorption capacity of SBCs in ecologically and climatically different
418 soils, so as to establish a database of PTE immobilization capacity of SBCs in soils.

419

420 **Acknowledgements**

421 This work was financially supported by the National Key Research and Development Program of China
422 (2017YFD0202101), the National Natural Science Foundation of China (21866013, 21876027), the United
423 Fund of Guangdong Provincial Basic and Applied Basic Research Foundation, China (2019A1515110705), the
424 Crop Science Postgraduate Innovation Project of Hainan University Tropical Agriculture and Forestry College,
425 China (ZWCX2018012, ZWCX2018013), and the Special Fund for the Science and Technology Innovation
426 Team of Foshan, China (1920001000083).

427

428 **References**

429 Ali, S., Rizwan, M., Shakoor, M.B., Jilani, A., Anjum, R., 2020. High sorption efficiency for As(III) and As(V) from aqueous
430 solutions using novel almond shell biochar, *Chemosphere.* 243, 125330.
431 <https://doi.org/10.1016/j.chemosphere.2019.125330>

432 Andreas, R., Zhang, J., 2014. Characteristics of adsorption interactions of cadmium(II) onto humin from peat soil in
433 freshwater and seawater media. *B. Environ. Contam. Tox.* 92, 352–357. <https://doi.org/10.1007/s00128-014-1205-x>

434 Bandara, T., Franks, A., Xu, J., Bolan, N., Wang, H., Tang, C., 2020. Chemical and biological immobilization mechanisms of
435 potentially toxic elements in biochar-amended soils. *Crit. Rev. Environ. Sci. Technol.* 50, 903-978.
436 [doi:10.1080/10643389.2019.1642832](https://doi.org/10.1080/10643389.2019.1642832)

437 Bao, S., 2000. *Chemical Analysis for Agricultural Soil*. China Agriculture Press, Beijing.

438 Batrusaitis, J., Chen, H.H., Rubasinghege, G., Grassian, V.H., 2012. Heterogeneous atmospheric chemistry of lead oxide
439 particles with nitrogen dioxide increases lead solubility: environmental and health implications. *Environ. Sci. Technol.*
440 46 (23), 12806–12813. <https://doi.org/10.1021/es3019572>

441 Bennett, L.T., Hinko-Najera, N., Aponte, C., Nitschke, C.R., Fairman, T.A., Fedrigo, M., Kasel, S., 2020. Refining
442 benchmarks for soil organic carbon in Australia’s temperate forests. *Geoderma* 368, 11424.
443 <https://doi.org/10.1016/j.geoderma.2020.114246>

444 Boehm, H.P., 1994. Some aspects of the surface chemistry of carbon blacks and other carbons. *Carbon* 32 (5), 759–769.
445 [https://doi.org/10.1016/0008-6223\(94\)90031-0](https://doi.org/10.1016/0008-6223(94)90031-0)

446 Brunauer, S., Emmett, P.H., Teller, E., 1938. Adsorption of gases in multimolecular layers. *J. Am. Chem. Soc.* 60 (2),
447 309–319. <https://doi.org/10.1021/ja01269a023>

448 Cao, Y., Jing, Y., Hao, H., Wang, X., 2019. Changes in the physicochemical characteristics of peanut straw biochar after
449 freeze-thaw and dry-wet aging treatments of the biomass. *BioResources* 14(2), 4329–4343.
450 <https://doi.org/10.15376/biores.14.2.4329-4343>

451 Chen, H., Yang, X., Wang, H., Sarkar, B., Shaheen, S.M., Gielen, G., Bolan, N., Guo, J., Che, L., Sun, H., Rinklebe, J., 2020a.
452 Animal carcass- and wood-derived biochars improved nutrient bioavailability, enzyme activity, and plant growth in
453 metal-phthalic acid ester co-contaminated soils: A trial for reclamation and improvement of degraded soils. *Journal of*

454 Environmental Management 261, 110246. <https://doi.org/10.1016/j.jenvman.2020.110246>

455 Chen, Y., Lee, S., Tahmasebi, A., Bai, J., Vongsvivut, J., Yu, J., 2020b. Chemical structure transformation during the later
456 stage of plastic layers during coking using Synchrotron infrared microspectroscopy technique. *Fuel*. 273, 117764.
457 <https://doi.org/10.1016/j.fuel.2020.117764>

458 Cheng, C.-H., Lehmann, J., Engelhard, M.H., 2008. Natural oxidation of black carbon in soils: Changes in molecular form
459 and surface charge along a climosequence. *Geochim. Cosmochim. Ac.* 72, 1598–1610.
460 <https://doi.org/10.1016/j.gca.2008.01.010>

461 Chiou, C.T., 2002. Partition and Adsorption of Organic Contaminants in Environmental Systems. Wiley-Interscience.
462 [https://doi.org/10.1016/S0304-3894\(02\)00361-8](https://doi.org/10.1016/S0304-3894(02)00361-8)

463 D1762-84, 2007. Standard Test Method for Chemical Analysis of Wood Charcoal. American Society for Testing and
464 Materials, Conshohocken, PA.

465 Deng, J., Liu, Y., Liu, S., Zeng, G., Tan, X., Huang, B., Tang, X., Wang, S., Hua, Q., Yan, Z., 2017. Competitive adsorption
466 of Pb(II), Cd(II) and Cu(II) onto chitosan-pyromellitic dianhydride modified biochar. *J. Colloid. Interface. Sci.* 506,
467 355–364. <https://doi.org/10.1016/j.jcis.2017.07.069>

468 Dodson, J., Li, J., Lu, F., Zhang, W., Yan, H., Cao, S., 2019. A late pleistocene and holocene vegetation and environmental
469 record from shuangchi maar, hainan province, South China. *Palaeogeogr. Palaeocl.* 523, 89–96.
470 <https://doi.org/10.1016/j.palaeo.2019.03.026>

471 Dong, X., Li, G., Lin, Q., Zhao, X., 2017. Quantity and quality changes of biochar aged for 5 years in soil under field
472 conditions. *Catena* 159, 136–143. <https://doi.org/10.1016/j.catena.2017.08.008>

473 Fang, Z., Gao, Y., Bolan, N., Shaheen, S.M., Xu, S., Wu, X., Xu, X., Hu, H., Lin, J., Zhang, F., Li, J., Rinklebe, J., Wang, H.,
474 2020. Conversion of biological solid waste to graphene-containing biochar for water remediation: A critical review.
475 *Chem. Eng. J.* 390, 124611. <https://doi.org/10.1016/j.cej.2020.124611>

476 Hardy, B., Leifeld, J., Knicker, H., Dufey, J.E., Deforce, K., Cornélias, J.T., 2017. Long term change in chemical properties of
477 preindustrial charcoal particles aged in forest and agricultural temperate soil. *Org. Geochem.* 107, 33–45.
478 <https://doi.org/10.1016/j.orggeochem.2017.02.008>

479 Imran, M., Khan, Z.U.H., Iqbal, J., Shah, N.S., Muzammil, S., Ali, S., Muhammad, N., Aziz, A., Murtaza, B., Naeem, M.A.,
480 Amjad, M., Shahid, M., Zakir, A., Rizwan, M., 2020. Potential of siltstone and its composites with biochar and
481 magnetite nanoparticles for the removal of cadmium from contaminated aqueous solutions: Batch and column scale
482 studies, *Environ. Pollut.* 259, 113938. <https://doi.org/10.1016/j.envpol.2020.113938>

483 Jaffé, R., Ding, Y., Niggemann, J., Vähätalo, A. V, Stubbins, A., Spencer, R.G.M., Campbell, J., Dittmar, T., 2013. Global
484 charcoal mobilization from soils via dissolution and riverine transport to the oceans. *Science* 340, 345–347.
485 <https://doi:10.1126/science.1231476>

486 Koide, R. T., Petprakob, K., Peoples, M., 2011. Quantitative analysis of biochar in field soil. *Soil Biol. Biochem.* 43,
487 1563–1568. <https://doi.org/10.1016/j.soilbio.2011.04.006>

488 Lehmann, J., Liang, B., Solomon, D., Lerotic, M., Luizão, F., Kinyangi, J., Schäfer, T., Wirrick, S., Jacobsen, C., 2005.
489 Near-edge X-ray absorption fine structure (NEXAFS) spectroscopy for mapping nano-scale distribution of organic
490 carbon forms in soil: Application to carbon particles. *Global. Biogeochem. Cy.* 19,
491 <https://doi.org/10.1029/2004GB002435>

492 Li, J., Wang, S.-L., Zhang, J., Zheng, L., Chen, D., Wu, Z., Shaheen, S.M., Rinklebe, J., Ok, Y.S., Wang, H., Wu, W., 2020.
493 Coconut-fiber biochar reduced the bioavailability of lead but increased its translocation rate in rice plants: Elucidation
494 of immobilization mechanisms and significance of iron plaque barrier on roots using spectroscopic techniques. *J.*
495 *Hazard. Mater.* 389, 122117. <https://doi.org/10.1016/j.jhazmat.2020.122117>

496 Li, J., Wang, S.-L., Zheng, L., Chen, D., Wu, Z., Xie, Y., Wu, W., Niazi, N.K., Ok, Y.S., Rinklebe, J., Wang, H., 2019a.
497 Sorption of lead in soil amended with coconut fiber biochar: Geochemical and spectroscopic investigations. *Geoderma*

498 350, 52–60. <https://doi.org/10.1016/j.geoderma.2019.05.008>

499 Li, J., Zheng, L., Wang, S.-L., Wu, Z., Wu, W., Niazi, N.K., Shaheen, S.M., Rinklebe, J., Bolan, N., Ok, Y.S. Wang, H.,
500 2019b. Sorption mechanisms of lead on silicon-rich biochar in aqueous solution: Spectroscopic investigation. *Sci.*
501 *Total Environ.* 672, 572–582. <https://doi.org/10.1016/j.scitotenv.2019.04.003>

502 Liang, B., Lehmann, J., Solomon, D., Kinyangi, J., Grossman, J., O'Neill, B., Skjemstad, J. O., Thies, J., Luizão, F. J.,
503 Petersen, J., 2006. Black carbon increases cation exchange capacity in soil. *Soil. Sci. Soc. Am. J.* 70, 1719–1730.
504 <https://doi.org/10.2136/sssaj2005.0383>

505 Liang, B., Lehmann, J., Solomon, D., Sohi, S., Thies, J. E., Skjemstad, J. O., Luizão, F. J., Engelhard, M. H., Neves, E. G.,
506 Wirrick, S., 2008. Stability of biomass-derived black carbon in soils. *Geochim. Cosmochim. Ac.* 72, 6069–6078.
507 <https://doi.org/10.1016/j.gca.2008.09.028>

508 Liu, H., Xu, F., Xie, Y., Wang, C., Zhang, A., Li, L., Xu, H., 2018. Effect of modified coconut shell biochar on availability of
509 heavy metals and biochemical characteristics of soil in multiple heavy metals contaminated soil. *Sci. Total Environ.*
510 645, 702–709. <https://doi.org/10.1016/j.scitotenv.2018.07.115>

511 Lu, H., Zhang, W., Yang, Y., Huang, X., Wang, S., Qiu, R., 2012. Relative distribution of Pb²⁺ sorption mechanisms by
512 sludge-derived biochar. *Water. Res.* 46, 854–862. <https://doi.org/10.1016/j.watres.2011.11.058>.

513 Lu, K., Yang, X., Gielen, G., Bolan, N., Ok, Y.S., Niazi, N.K., Xu, S., Yuan, G., Chen, X., Zhang, X., Liu, D., Song, Z., Liu,
514 X., Wang, H., 2017. Effect of bamboo and rice straw biochars on the mobility and redistribution of heavy metals (Cd,
515 Cu, Pb and Zn) in contaminated soil. *J. Environ.Manag.* 186, 285–292. <https://doi.org/10.1016/j.jenvman.2016.05.068>.

516 Lu, X., Zang, R., Ding, Y., Huang, J., 2018. Partitioning the functional variation of tree seedlings during secondary
517 succession in a tropical lowland rainforest. *Ecosphere* 9(6), e02305. <https://doi.org/10.1002/ecs2.2305>

518 Mia, S., Dijkstra, F.A., Singh, B., 2017. Chapter one – long-term aging of biochar: a molecular understanding with
519 agricultural and environmental implications. *Adv. Agron.* 141, 1–51. <https://doi.org/10.1016/bs.agron.2016.10.001>

520 Mukherjee, A., Zimmerman, A.R., Cooper, W.T., Hamdan, R., 2014. Physicochemical changes in pyrogenic organic matter
521 (biochar) after 15 months of field aging. *Solid Earth* 5(2), 693–704. <https://doi.org/10.5194/se-5-693-2014>

522 Mumtaz, I., Majeed, Z., Ajab, Z., Ahmad, B., Khurshid, K., Mubashir, M., 2019. Optimized tuning of rosin adduct with
523 maleic anhydride for smart applications in controlled and targeted delivery of urea for higher plant's uptake and growth
524 efficiency. *Ind. Crop. Prod.* 133, 395–408. <https://doi.org/10.1016/j.indcrop.2019.02.036>

525 Ngambia, A., Ifthikar, J., Shahib, I. I., Jawad, A., Shahzad, A., Zhao, M., Wang, J., Chen, Z., Chen, Z., 2019. Adsorptive
526 purification of heavy metal contaminated wastewater with sewage sludge derived carbon-supported Mg(II) composite.
527 *Sci. Total Environ.* 691, 306–321. <https://doi.org/10.1016/j.scitotenv.2019.07.003>

528 Nie, C., Yang, X., Niazi, N.K., Xu, X., Wen, Y., Rinklebe, J., Ok, Y.S., Xu, S., Wang, H., 2018. Impact of sugarcane
529 bagasse-derived biochar on heavy metal availability and microbial activity: A field study. *Chemosphere* 200,
530 274-282. <https://doi.org/10.1016/j.chemosphere.2018.02.134>

531 Nolan, R.H., Boer, M.M., Collins, L., Resco de Dios, V., Clarke, H., Jenkins, M., Kenny, B., Bradstock, R.A., 2020. Causes
532 and consequences of eastern Australia's 2019–20 season of mega-fires. *Global Change Biol.* 26(3), 1039–1041.
533 <https://doi.org/10.1111/GCB.14987>

534 Pereira, R.C., Arbestain, M.C., Kaal, J., Sueiro, M.V., Sevilla, M., Hindmarsh, J., 2014. Detailed carbon chemistry in
535 charcoals from pre-European Maori gardens of New Zealand as a tool for understanding biochar stability in soils. *Eur.*
536 *J. Soil Sci.* 65, 83–95. <https://doi.org/10.1111/ejss.12096>

537 Plante, A. F., Fernández, J. M., Leifeld, J., 2009. Application of thermal analysis techniques in soil science. *Geoderma*
538 153(1–2), 1–10. <https://doi.org/10.1016/j.geoderma.2009.08.016>

539 Qi, F.J., Kuppusamy, S., Naidu, R., Bolan, N.S., Ok, Y.S., Lamb, D., Li, Y.B., Yu, L.B., Semple, K.T., Wang, H.L., 2017.
540 Pyrogenic carbon and its role in contaminant immobilization in soils. *Critical Reviews in Environmental Science and*
541 *Technology* 47, 795-876. doi:10.1080/10643389.2017.1328918

542 Qin, P., Wang, H., Yang, X., He, L., Müller, K., Shaheen, S.M., Xu, S., Rinklebe, J., Tsang, D.C.W., Ok, Y.S., Bolan, N.,
543 Song, Z., Che, L., Xu, X., 2018. Bamboo- and pig-derived biochars reduce leaching losses of dibutyl phthalate,
544 cadmium, and lead from co-contaminated soils. *Chemosphere* 198, 450-459.
545 <https://doi.org/10.1016/j.chemosphere.2018.01.162>

546 Schmidt, M.W.I., Noack, A.G., 2000. Black carbon in soils and sediments: Analysis, distribution, implications, and current
547 challenges. *Global Biogeochem. Cy.* 14, 777–793. <https://doi.org/10.1029/1999GB001208>

548 Uzun, H., Bayhana, Y.K., Kaya, Y., Cakici, A., Algur, O.F., 2003. Biosorption of lead (II) from aqueous solution by cone
549 biomass of *Pinus sylvestris*. *Desalination* 154, 233–238. [https://doi.org/10.1016/s0011-9164\(03\)80038-3](https://doi.org/10.1016/s0011-9164(03)80038-3)

550 Wang, C., Liu, J., Shen, J., Chen, D., Li, Y., Jiang, B., Wu, J., 2018. Effects of biochar amendment on net greenhouse gas
551 emissions and soil fertility in a double rice cropping system: a 4-year field experiment. *Agr. Ecosyst. Environ.* 262,
552 83–96. <https://doi.org/10.1016/j.agee.2018.04.017>

553 Wang, H., Gao, B., Wang, S., Fang, J., Xue, Y., Kai, Y., 2015. Removal of Pb(II), Cu(II), and Cd(II) from aqueous solutions
554 by biochar derived from KMnO₄ treated hickory wood. *Bioresour. Technol.* 197, 356–362.
555 <https://doi.org/10.1016/j.biortech.2015.08.132>

556 Wang, J., Ren, C., Cheng, H., Zou, Y., Bughio, M. A., Li, Q., 2017a. Conversion of rainforest into agroforestry and
557 monoculture plantation in China: consequences for soil phosphorus forms and microbial community. *Sci. Total*
558 *Environ.* 595, 769–778. <https://doi.org/10.1016/j.scitotenv.2017.04.012>

559 Wang, L., Wang, Y., Ma, F., Tankpa, V., Bai, S., Guo, X., Wang, X., 2019. Mechanisms and reutilization of modified biochar
560 used for removal of heavy metals from wastewater: A review. *Sci. Total Environ.* 668, 1298–1309.
561 <https://doi.org/10.1016/j.scitotenv.2019.03.011>

562 Wang, X., Miao, H., He, W., Shen, H., 2011. Competitive adsorption of Pb(II), Cu(II), and Cd(II) ions on wheat-residue
563 derived black carbon. *J. Chem. Eng. Data* 56(3), 444–449. <https://doi.org/10.1021/je101079w>

564 Wei, J., Tu, C., Yuan, G., Zhou, Y., Wang, H., Lu, J., 2020. Limited Cu(II) binding to biochar DOM: Evidence from C K-edge
565 NEXAFS and EEM-PARAFAC combined with two-dimensional correlation analysis. *Science of The Total*
566 *Environment* 701, 134919. <https://doi.org/10.1016/j.scitotenv.2019.134919>

567 Wu, W., Li, J., Lan, T., Müller, K., Niazi, N. K., Chen, X., Xu, S., Zheng, L., Chu, Y., Li, J., 2017. Unraveling sorption of
568 lead in aqueous solutions by chemically modified biochar derived from coconut fiber: A microscopic and spectroscopic
569 investigation. *Sci. Total Environ.* 576, 766–774. <https://doi.org/10.1016/j.scitotenv.2016.10.163>.

570 Wu, W., Li, J., Niazi, N. K., Müller, K., Chu, Y., Zhang, L., Yuan, G., Lu, K., Song, Z., Wang, H., 2016. Influence of
571 pyrolysis temperature on lead immobilization by chemically modified coconut fiber-derived biochars in aqueous
572 environments. *Environ. Sci. Pollut. Res.* 23, 22890–22896. <https://doi.org/10.1007/s11356-016-7428-0>.

573 Wu, W., Yang, M., Feng, Q., McGrouther, K., Wang, H., Lu, H.H., Chen, Y.X., 2012. Chemical characterization of rice
574 straw-derived biochar for soil amendment. *Biomass Bioenergy* 47, 268–276.
575 <https://doi.org/10.1016/j.biombioe.2012.09.034>.

576 Xia, Y., Yang, T., Zhu, N., Li, D., Chen, Z., Lang, Q., Liu, Z., Jiao, W., 2019. Enhanced adsorption of Pb (II) onto modified
577 hydrochar: modeling and mechanism analysis. *Bioresour. Technol.* 121593.
578 <https://doi.org/10.1016/j.biortech.2019.121593>

579 Xin, X., Qin, W., Jian, Y., Yan, L., Rui, F., Chen, G., Du, B., He, L., 2012. Highly efficient removal of heavy metal ions by
580 amine-functionalized mesoporous Fe₃O₄ nanoparticles. *Chem. Eng. J.* 184, 132–140.
581 <https://doi.org/10.1016/j.cej.2012.01.016>

582 Yamada, Y., Suzuki, Y., Yasuda, H., Uchizawa, S., Hirose-Takai, K., Sato, Y., Suenaga, K., Sato, S., 2014. Functionalized
583 graphene sheets coordinating metal cations. *Carbon* 75, 81–94. <https://doi.org/10.1016/j.carbon.2014.03.036>

584 Yang, X., Wan, Y., Zheng, Y., He, F., Yu, Z., Huang, J., Wang, H., Ok, Y.S., Jiang, Y., Gao, B., 2019. Surface functional
585 groups of carbon-based adsorbents and their roles in the removal of heavy metals from aqueous solutions: A critical

586 review. *Chem. Eng. J.* 366, 608–621. <https://doi.org/10.1016/j.cej.2019.02.119>

587 Yin, G., Song, X., Tao, L., Sarkar, B., Sarmah, A.K., Zhang, W., Lin, Q., Xiao, R., Liu, Q., Wang, H., 2020. Novel Fe-Mn
588 binary oxide-biochar as an adsorbent for removing Cd(II) from aqueous solutions. *Chemical Engineering Journal* 389,
589 124465. <https://doi.org/10.1016/j.cej.2020.124465>

590 Zahedifar, M., 2017. Sequential extraction of zinc in the soils of different land use types as influenced by wheat straw
591 derived biochar. *J. Geochem. Explor.* 182, 22–31. <https://doi.org/10.1016/j.gexplo.2017.08.007>

592 Zhang, J., Shao, J., Jin, Q., Li, Z., Zhang, X., Chen, Y., Zhang, S., Chen, H., 2019. Sludge-based biochar activation to
593 enhance Pb (II) adsorption. *Fuel* 252, 101–108. <https://doi.org/10.1016/j.fuel.2019.04.096>

594 Zhang, M., Fellowes, J. R., Jiang, X., Wang, W., Chan, B. P. L., Ren, G., Zhu, J. G., 2010. Degradation of tropical forest in
595 Hainan, China, 1991-2008: conservation implications for hainan gibbon (*nomascus hainanus*). *Biol. Conserv.* 6(143),
596 1397–1404. <https://doi.org/10.1016/j.biocon.2010.03.014>

597 Zhang, Q., Yang, Q., Phanlavong, P., Li, Y., Peng, Q., 2017. Highly efficient lead(II) sequestration using size-controllable
598 polydopamine microspheres with superior application capability and rapid capture. *Acs Sustain. Chem. Eng.* 5,
599 4161–4170. <https://doi.org/10.1021/acssuschemeng.7b00129>

600 Zhang, X., Gao, B., Fang, J., Zou, W., Dong, L., Cao, C., Zhang, J., Li, Y., Wang, H., 2019. Chemically activated hydrochar
601 as an effective adsorbent for volatile organic compounds (VOCs). *Chemosphere* 218, 680-686.
602 <https://doi.org/10.1016/j.chemosphere.2018.11.144>

603 Zhou, T., Wu, L., Luo, Y., Christie, P., 2018. Effects of organic matter fraction and compositional changes on distribution of
604 cadmium and zinc in long-term polluted paddy soils. *Environ. Pollut.* 232, 1–9.
605 <https://doi.org/10.1016/j.envpol.2017.09.081>

606

607

608 **Figure captions**

609 **Fig. 1.** The FTIR spectra of SBC samples.

610 **Fig. 2.** Isotherms of Pb sorption on SBCs.

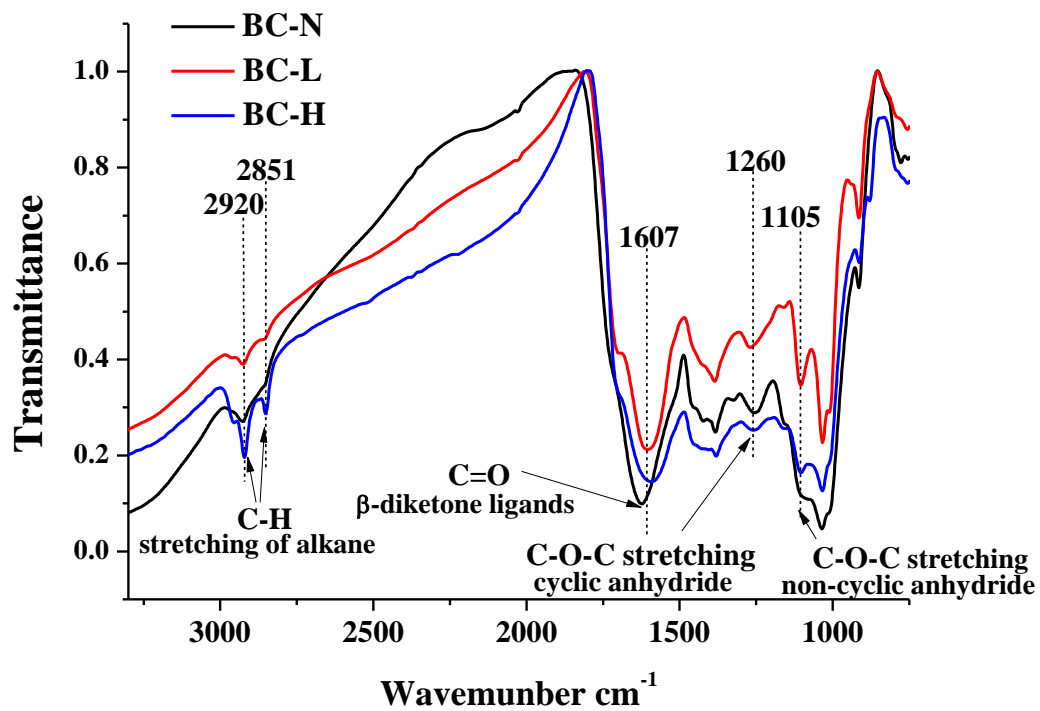
611 **Fig. 3.** Total Pb amounts and Pb amounts of four fractions on the three Pb-loaded SBCs prepared under increasing initial
612 concentration of Pb.

613 **Fig. 4.** Amounts of Pb in different Pb fractions on Pb-loaded SBCs under Pb concentration of 1000 mg L⁻¹.

614 **Fig. 5.** XPS wide scan spectra of Pb 4f, C 1s and O 1s (a), high-resolution spectra of Pb 4f region (b), and high-resolution
615 spectra of C 1s regions (c–h) on SBCs before and after Pb sorption.

616

617

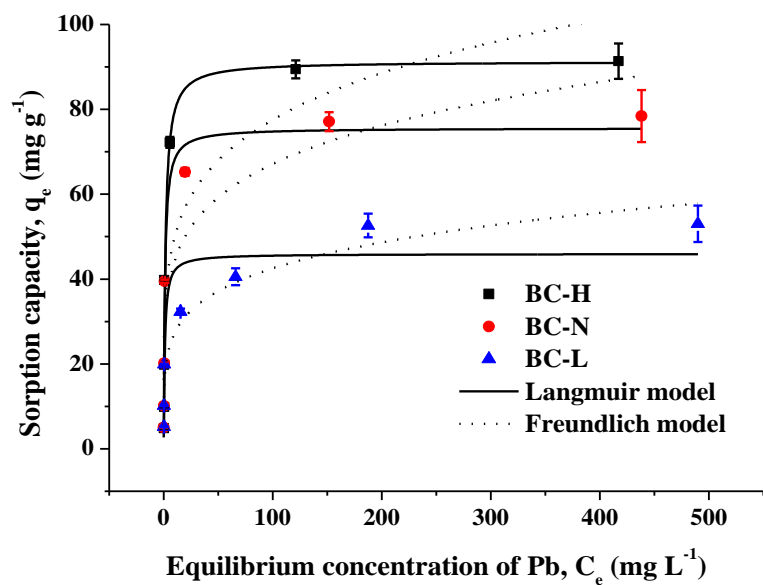


618

619 **Fig. 1.** The FTIR spectra of SBC samples, the sample ID of BC-N, BC-L and BC-H refer to SBC selected from Soil 1, Soil 2

620 and Soil 3, respectively.

621

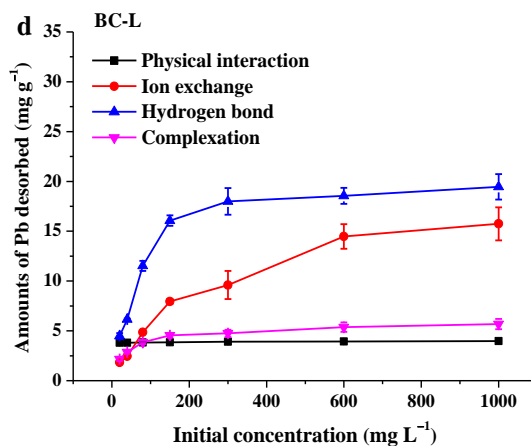
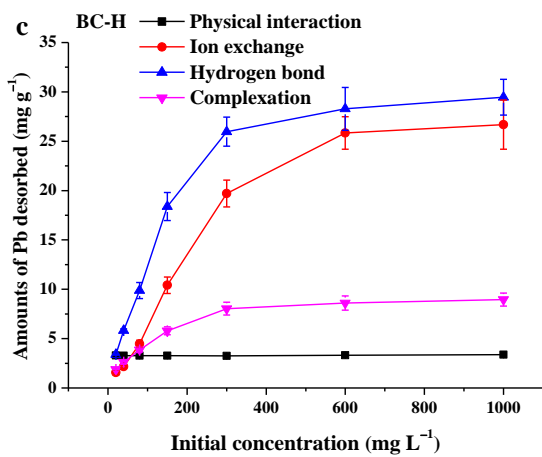
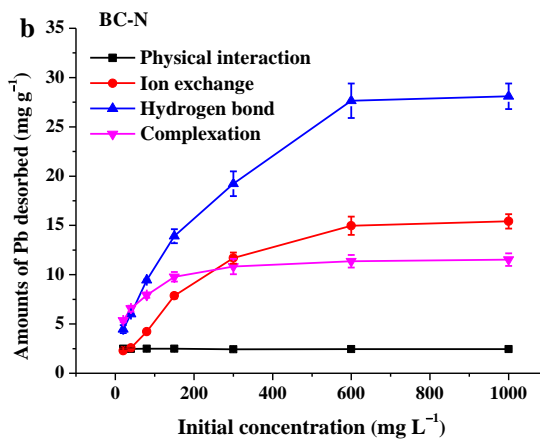
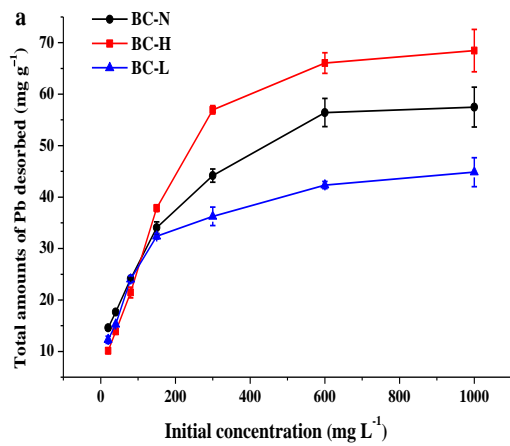


622

623

Fig. 2. Isotherms of Pb sorption on SBCs.

624



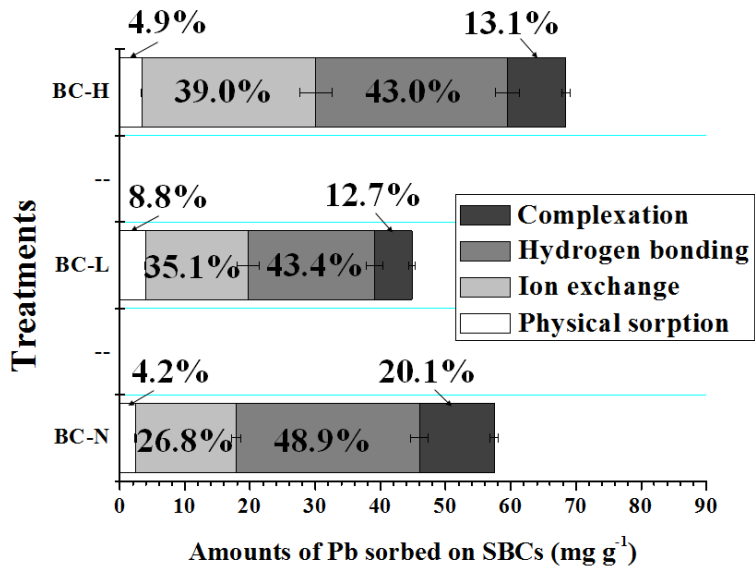
625

626

627 **Fig. 3.** Total Pb amounts and Pb amounts of four fractions on the three Pb-loaded SBCs prepared under increasing initial

628 concentration of Pb.

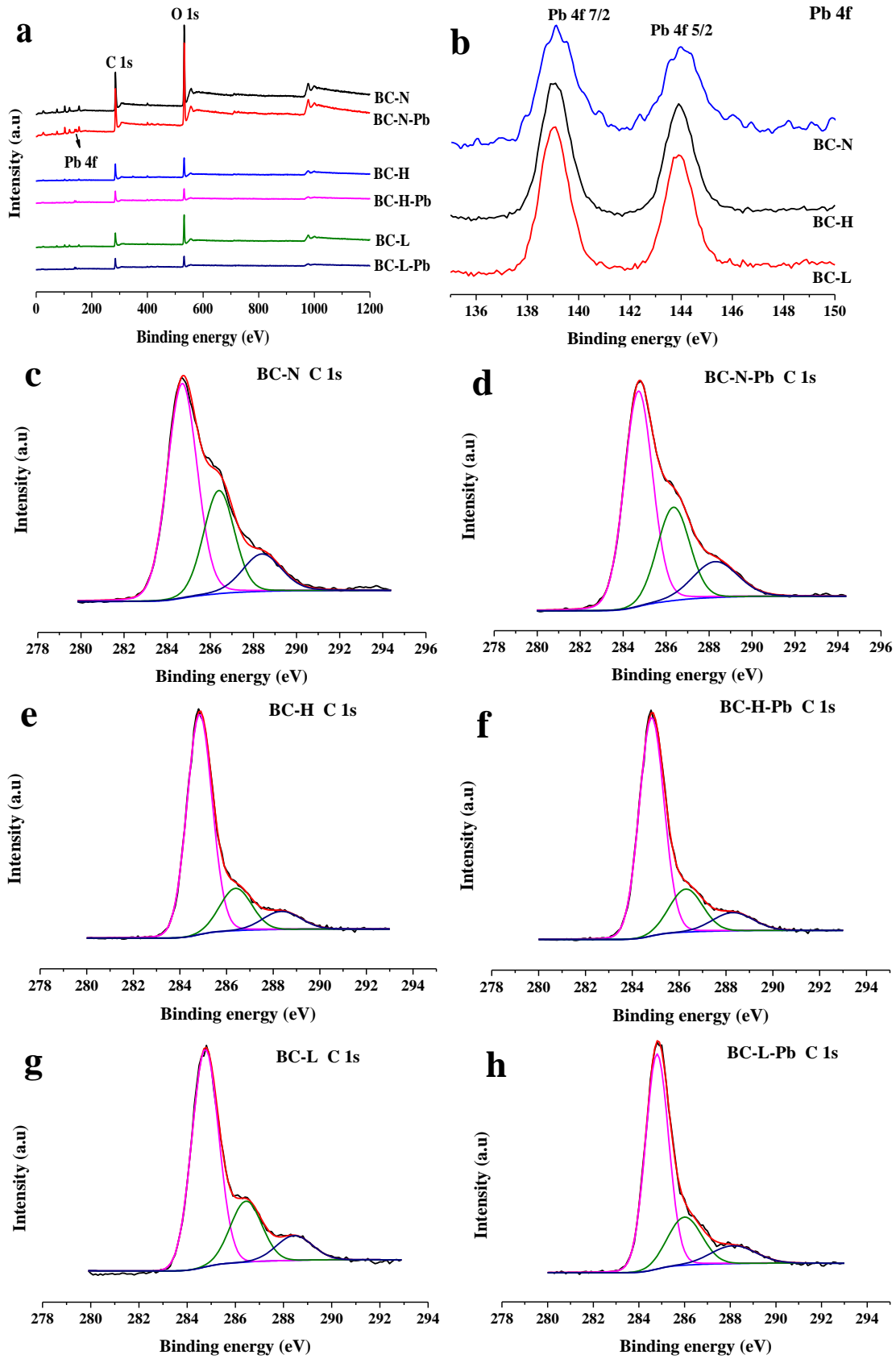
629



630

631 **Fig. 4.** Amounts of Pb in different Pb fractions on Pb-loaded SBCs under Pb concentration of 1000 mg L⁻¹.

632



633

634

635

636

637

638

639

Fig. 5. XPS wide scan spectra of Pb 4f, C 1s and O 1s (a), high-resolution spectra of Pb 4f region (b), and high-resolution spectra of C 1s regions (c–h) on SBCs before and after Pb sorption.

640 **Table 1.** Composition and selected properties of SBCs.

Sample ID	Elemental component (%)				Atomic ratio			n(RCOOH)	n(RCOR')	n(AOH)	CEC	SSA (m ² g ⁻¹)
	C	H	N	O	H/C	O/C	(O+N)/C	(mmol g ⁻¹)	(mmol g ⁻¹)	(mmol g ⁻¹)	(cmol kg ⁻¹)	
BC-N	49.1	3.61	0.73	46.5	0.88	0.71	0.72	0.53 ± 0.02	0.70 ± 0.03	0.34 ± 0.04	128.0 ± 24.9	7.51 ± 1.1
BC-L	47.9	3.87	1.64	46.6	0.97	0.73	0.76	0.49 ± 0.01	1.13 ± 0.19	0.09 ± 0.01	166.4 ± 13.4	34.1 ± 2.7
BC-H	45.9	3.90	2.36	47.8	1.02	0.78	0.83	0.03 ± 0.01	0.64 ± 0.03	1.03 ± 0.01	227.3 ± 11.7	20.3 ± 1.8

641 Notes: Results are means ± SD (n = 3), the sample ID of BC-N, BC-L and BC-H refer to SBC selected and picked from Soil 1 (no-cultivation), Soil 2 (less intensive cultivation) and Soil 3

642 (highly intensive cultivation), respectively. While the RCOOH, RCOR', and AOH refer to carboxylic acid, weak acid ester, and phenolic hydroxyl groups, respectively.

643 **Table 2.** Peak positions and relative contents of surface functional groups determined from C 1s and O 1s XPS spectra for
 644 SBCs before and after Pb sorption.

Sample ID		Bonds and groups of C 1s			Bonds and groups of O 1s	
		C–C/C=C/C–H	C–O	C=O/O–C=O	C=O	C–O
BC-N	Beam energy (eV)	284.7	286.4	288.4	531.9	532.8
	Atomic percentage (%)	58.2	28.3	13.6	59.7	40.3
BC-N-Pb	Beam energy (eV)	284.7	286.3	288.3	532	532.8
	Atomic percentage (%)	57.4	27.5	15.1	62.3	37.7
BC-L	Beam energy (eV)	284.7	286.4	288.4	532	532.9
	Atomic percentage (%)	67.5	22.2	10.3	61.8	38.2
BC-L-Pb	Beam energy (eV)	284.7	286.3	288.3	531.8	532.8
	Atomic percentage (%)	67.7	21.8	10.5	62.4	37.6
BC-H	Beam energy (eV)	284.8	286.3	288.3	531.9	532.7
	Atomic percentage (%)	73.2	19.3	7.5	64.5	35.5
BC-H-Pb	Beam energy (eV)	284.8	286.3	288.3	531.9	533.2
	Atomic percentage (%)	72	18.5	9.5	77.4	22.6

645

646

647 **Supplementary Material:**

648 **Sorption mechanisms of lead on soil-derived black carbon**
649 **formed under varying cultivation systems**

650

651 **Qingjie Zhao ^{a,1}, Jianhong Li ^{a,b,1}, Binoy Sarkar ^c, Weidong Wu ^a, Boling Li ^a, Ruichun Liu ^d, Mohsin**
652 **Nawaz ^e, Muhammad Zia-ur-Rehman ^f, Hailong Wang ^{b,g,**}, Zhipeng Wu ^{a,*}**

653

654 ^a College of Tropical Crops, Hainan University, Haikou 570228, China

655 ^b Biochar Engineering Technology Research Center of Guangdong Province, School of Environmental and
656 Chemical Engineering, Foshan University, Foshan 528000, China

657 ^c Lancaster Environment Centre, Lancaster University, Lancaster, LA1 4YQ, United Kingdom

658 ^d Flood Control and Drought Relief Office of Hangjin County, Ordos 017400, China

659 ^e Key Laboratory of Genetics and Germplasm Innovation of Tropical Special Forest Trees and Ornamental
660 Plants, Ministry of Education, College of Forestry, Hainan University, Haikou 570228, China

661 ^f Institute of Soil and Environmental Sciences, University of Agriculture, Faisalabad, 38040, Pakistan

662 ^g Key Laboratory of Soil Contamination Bioremediation of Zhejiang Province, Zhejiang A&F University,
663 Hangzhou 311300, China

664

665 * Corresponding author.

666 ** Correspondence to: H. Wang, School of Environmental and Chemical Engineering, Foshan University,
667 Foshan 528000, China

668 E-mail addresses: hailong.wang@fosu.edu.cn (H. Wang), peter@hainanu.edu.cn (Z. Wu).

669 ¹ Qingjie Zhao and Jianhong Li contributed to the work equally and should be considered co-first authors.

670

671 **Text S1.**

672 The pseudo-first-order (Eq. 1) and pseudo-second-order (Eq. 2) models used in this study:

673 $\ln(q_e - q_t) = \ln q_e - k_1 t$ 1

674 $t/q_t = 1/k_2 q_e^2 + 1/q_e$ 2

675 where, k_1 (h^{-1}) and k_2 ($h^{-1} \cdot (g \text{ mg}^{-1})$) are the rate constants of the pseudo first-order and pseudo-second order
676 models, respectively. While, q_e and q_t is the amount of Pb sorbed by SBC at equilibrium and at time (t) in $mg \text{ g}^{-1}$,
677 respectively.

678 The Langmuir (Eq. 3) and Freundlich (Eq. 4) models used in this study:

679 $q_e = q_{\max} K_L C_e / (1 + K_L C_e)$ 3

680 $q_e = K_f C_e^{1/n}$ 4

681 where, q_e ($mg \text{ g}^{-1}$) and C_e ($mg \text{ L}^{-1}$) are the amounts of Pb sorbed by SBC for a given initial Pb concentration,
682 and the concentration of Pb in solution at equilibrium, respectively. While, q_m ($mg \text{ g}^{-1}$) is the maximum amount
683 of Pb adsorbed at equilibrium, K_L ($L \text{ mg}^{-1}$) is the Langmuir constant; n and K_f ($(mg \text{ g}^{-1}) \cdot (mg \text{ L}^{-1})^{-n}$) are
684 equilibrium constants relating to sorption intensity and sorption capacity of the Freundlich model, respectively.

685

686 **Table S1.** Parameters of pseudo-first-order and pseudo-second-order kinetic models for Pb sorption on SBCs.

Sample ID	Pseudo-first-order			Pseudo-second-order		
	q_e (mg g ⁻¹)	k_1 (1 h ⁻¹)	r^2	q_e (mg g ⁻¹)	k_2 (g mg ⁻² h ⁻¹)	r^2
BC-N	31.18	7.22	0.795	32.92	0.356	0.998
BC-L	27.33	0.89	0.787	30.66	0.034	0.979
BC-H	49.11	13.19	0.992	50.63	0.592	0.999

687

Table S2. Parameters of Langmuir and Freundlich isotherm models for Pb sorption on SBCs.

Sample ID	Langmuir			Freundlich		
	q_m (mg g ⁻¹)	K_L (L mg ⁻¹)	r^2	K_f (mg ⁽¹⁻ⁿ⁾ L ⁿ g ⁻¹)	n	r^2
BC-N	75.6	0.916	0.981	29.11	0.182	0.847
BC-L	46.0	1.064	0.854	17.53	0.193	0.925
BC-H	91.3	0.675	0.920	32.13	0.191	0.728

688

689

690 **Table S3.** Sorption capacities of different biochars for removing Pb from aqueous solution at pH of 5.0.

Type of biochars	Metal ion	Q _m (mg g ⁻¹)	References
Oak bark char	Pb ²⁺	13.1	Mohan et al. 2007
Pomelo peel biochar	Pb ²⁺	88.7	Zhao et al., 2018
Coconut-fiber biochar	Pb ²⁺	79.4	Li et al., 2019
Raw sugarcane bagasse biochar	Pb ²⁺	81.9	Inyang et al., 2011
Corn stover biochar	Pb ²⁺	63.3	Li et al., 2018
Digested sugar beet biochar	Pb ²⁺	51.4	Inyang et al., 2012

691

692 **Table S4.** The parameters (r^2) of Langmuir model for different Pb fractions on Pb-loaded SBCs under increasing
693 initial Pb concentrations.

Sample ID	Physical interaction	Ion exchange	Hydrogen bond	Complexation	Total amount
BC-N	-	0.984	0.983	0.971	0.969
BC-L	-	0.986	0.968	0.979	0.987
BC-H	-	0.966	0.973	0.984	0.983

694

695 **Table S5.** Amounts of Pb in different fractions on Pb-loaded SBCs (prepared under Pb concentration of 1000 mg L⁻¹).

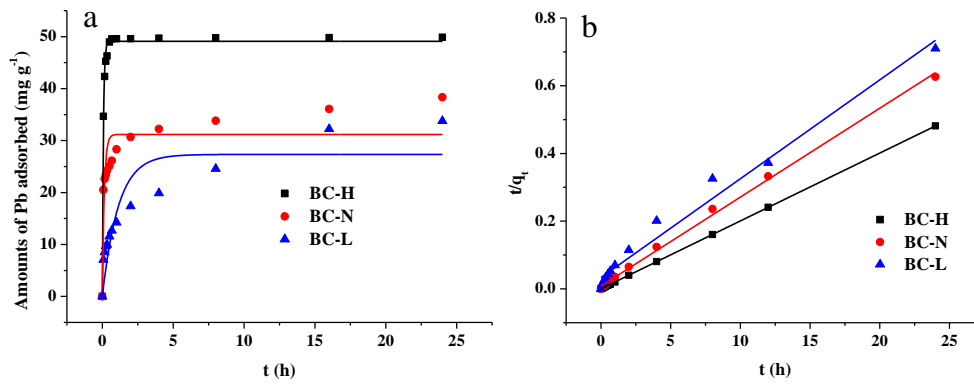
Sample ID	Amount of Pb in different fractions (mg g ⁻¹)				Total amount of desorption	Amount of sorbed Pb in a stable form in soil (mg kg ⁻¹) ^a
	Physical adsorption	Ion exchange	Hydrogen bonding	complexation		
BC-N	2.44	15.41	28.10	11.53	57.48	19.0
BC-L	3.97	15.74	19.45	5.68	44.84	18.7
BC-H	3.37	26.68	29.46	8.95	68.46	21.1

696 ^aThe amount of sorbed Pb in a stable form in soil (attribute to SBC sorption) was calculated by the equation: $Q_{sta} = M_{SBC} \times Q_{com}$, where Q_{sta} , M_{SBC} , and Q_{com} refer to the
 697 amount of stable Pb (in mg kg⁻¹), the content of SBC in soil (in g kg⁻¹), and amount of Pb in complexation fraction (in mg g⁻¹), respectively.

698 **Table S6.** Equivalents of adsorbed Pb by released cations from Pb-loaded SBCs.

Sample ID	K ⁺ (mg g ⁻¹)	Na ⁺ (mg g ⁻¹)	Ca ²⁺ (mg g ⁻¹)	Mg ²⁺ (mg g ⁻¹)
BC-N	1.32 ± 0.03	4.00 ± 0.96	7.12 ± 0.88	0.83 ± 0.01
BC-L	0.97 ± 0.12	2.03 ± 0.28	12.3 ± 1.78	0.33 ± 0.03
BC-H	0.98 ± 0.02	2.69 ± 0.44	14.5 ± 3.51	0.47 ± 0.01

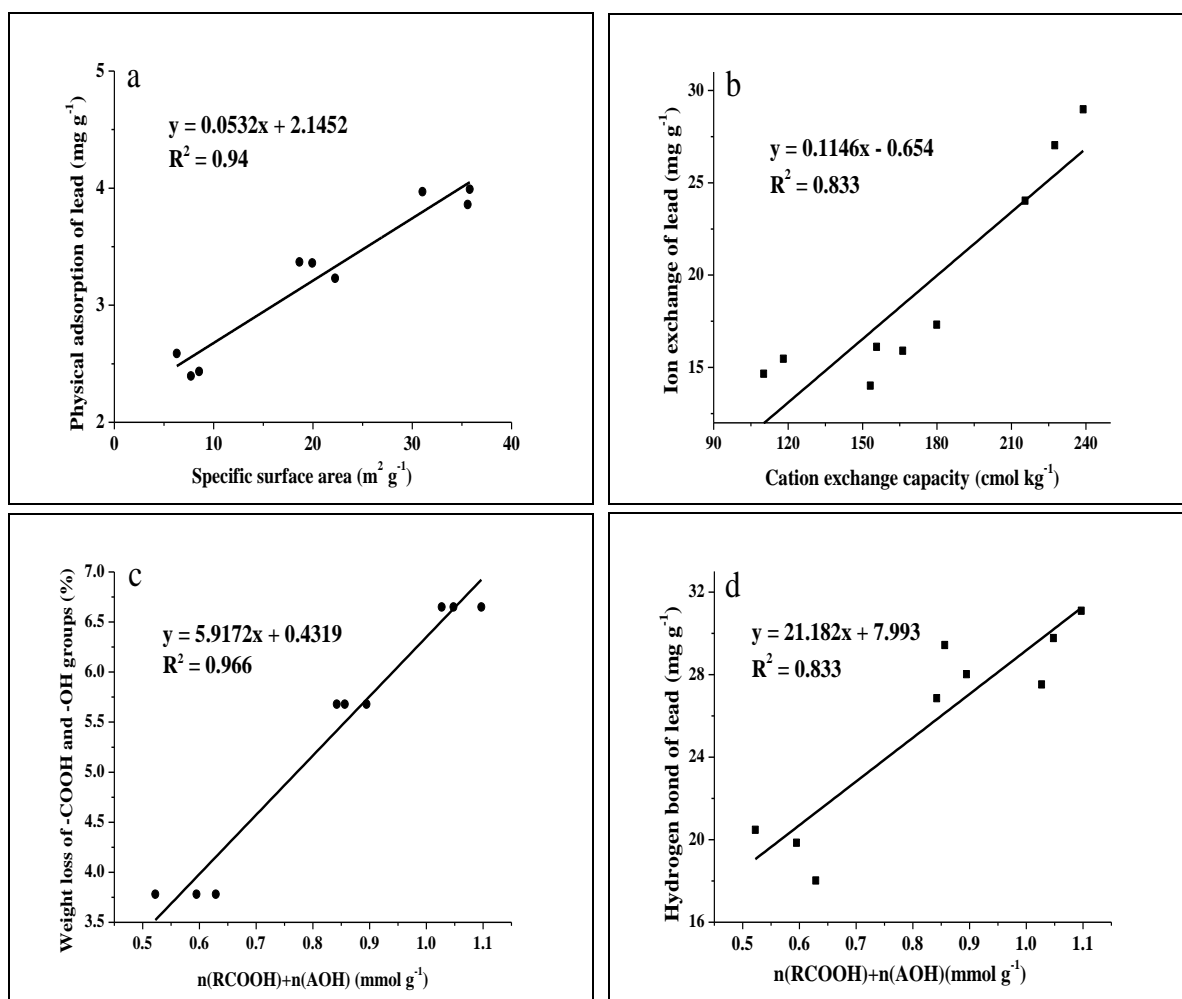
699



700

701 **Fig. S1.** Kinetics of Pb sorption on SBCs, a) pseudo-first-order kinetic
 702 model.

703

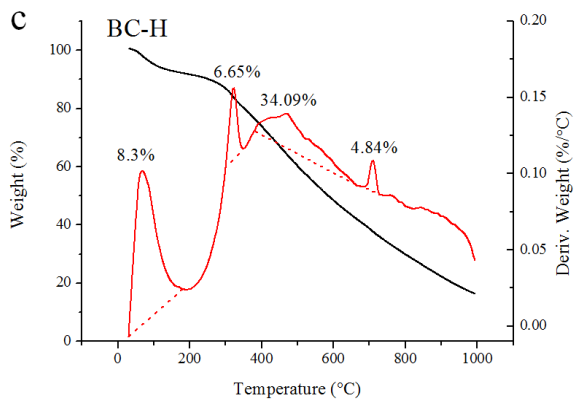
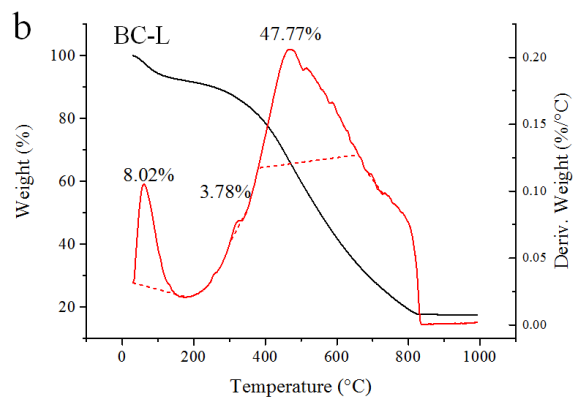
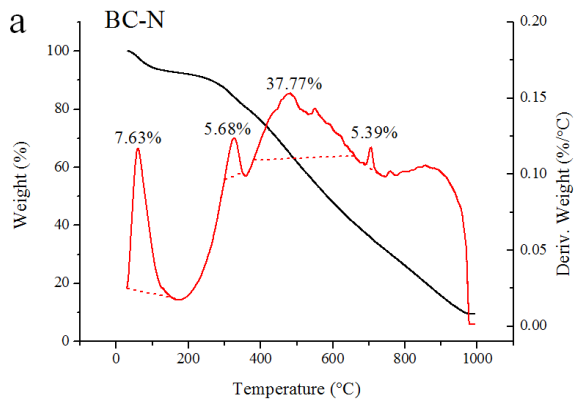


704

705

706 **Fig. S2.** Correlations between the amount of Pb in different fractions on Pb-loaded SBCs and specific properties
 707 of SBCs. a) physical adsorption fraction vs. specific surface area; b) ion exchange fraction vs. CEC; c) weight
 708 loss of -COOH and -OH groups on SBCs vs. the sum content of RCOOH and AOH functional groups on SBCs;
 709 and d) hydrogen bonding fraction vs. the sum content of RCOOH and AOH functional groups on SBCs.

710



711

712

713 Fig. S3. Thermogravimetric (TG, black line) and differential thermogravimetric (DTG, red line) curves of SBC samples: a)

714 BC-N, b) BC-L, and c) BC-H.

715

716 **References**

- 717 Inyang, M., Gao, B., Ding, W., Pullammanappallil, P., Zimmerman, A.R., Cao, X.D., 2011. Enhanced lead
718 sorption by biochar derived from anaerobically digested sugarcane bagasse. *Sep. Sci. Technol.* 46(12),
719 1950–1956. <https://doi.org/10.1080/01496395.2011.584604>
- 720 Inyang, M., Gao, B., Yao, Y., Xue, Y.W., Zimmerman, A.R., Pullammanappallil, P., Cao, X.D., 2012. Removal
721 of heavy metals from aqueous solution by biochars derived from anaerobically digested biomass. *Bioresour.*
722 *Technol.* 110, 50–56. <https://doi.org/10.1016/j.biortech.2012.01.072>
- 723 Li, C., Zhang, L., Gao, Y., Li, A., 2018. Facile synthesis of nano ZnO/ZnS modified biochar by directly
724 pyrolyzing of zinc contaminated corn stover for Pb(II), Cu(II) and Cr(VI) removals. *Waste. Manage.* 79,
725 525–637. <https://doi.org/10.1016/j.wasman.2018.08.035>
- 726 Li, J., Zheng, L., Wang, S.-L., Wu, Z., Wu, W., Niazi, N.K., Shaheen, S.M., Rinklebe, J., Bolan, N., Ok, Y.S.,
727 Wang, H., 2019. Sorption mechanisms of lead on silicon-rich biochar in aqueous solution: Spectroscopic
728 investigation. *Sci. Total Environ.* 672, 572-582. <https://doi.org/10.1016/j.scitotenv.2019.04.003>
- 729 Mohan, D., Pittman, C.U., Bricka, M., Smith, F., Yancey, B., Mohammad, J., Steele, P.H., Alexandre-Franco,
730 M.F., Gomez-Serrano, V., Gong, H., 2007. Sorption of arsenic, cadmium, and lead by chars produced from
731 fast pyrolysis of wood and bark during bio-oil production. *J. Colloid. Interf. Sci.* 310(1), 57–73.
732 <https://doi.org/10.1016/j.jcis.2007.01.020>
- 733 Zhao, T., Yao, Y., Li, D., Wu, F., Zhang, C., Gao, B., 2018. Facile low-temperature one-step synthesis of pomelo
734 peel biochar under air atmosphere and its adsorption behaviors for Ag(I) and Pb(II). *Sci. Total Environ.*
735 604–601, 73–79. <https://doi.org/10.1016/j.scitotenv.2018.05.251>
- 736